

# The $C_{60}^-$ thermal electron emission rate

K. Hansen<sup>1, \*</sup>

<sup>1</sup>*Center for Joint Quantum Studies and Department of Physics,  
School of Science, Tianjin University, 92 Weijin Road, Tianjin 300072, China*

(Dated: Monday 13<sup>th</sup> July, 2020, 01:30)

The thermal electron emission rate constant for  $C_{60}^-$  has been deduced over a range of 4 eV internal energy from storage ring measurements of the decays of ions reheated with single photons absorption. The thermal radiation from the ions is quantified with respect to continuous cooling and discrete photon quenching.

## I. INTRODUCTION

Measurements of rate constants in molecular beams with standard approaches require very good control over the excitation energy. A width in the internal energy distribution in a decaying particle or molecule will also introduce a width in the distribution of rate constants in the beam molecules, and due to the strong dependence of rate constants on excitation energy, any spread in energy is strongly amplified for the rate constants. This makes direct measurement of rate constants very difficult even for fairly narrow internal energy distributions. The problem is not solved by extracting molecules from canonical thermal distributions into molecular beams, as demonstrated in [1] with a calculation of a numerical example for  $C_{60}^-$ .

When the energy distribution of the molecules in a beam is sufficiently broad and in the absence of competing channels, molecular decay will occur with a rate with a time dependence close to  $1/t$  [2]. In the presence of the frequently occurring phenomenon of thermal radiation, this power law will be suppressed at long times with an almost exponential time dependence [3].

Situations with broad energy distributions arise particularly frequently for large molecules and clusters, because for these, excitation to internal energies where reactions occur on measurable time scales will require large amounts of energy, up to several tens of eV. Deposition of precise amounts of energies of such magnitudes is a very challenging experimental task. Photo excitation experiments with a single high energy photon, for example, will often lead to direct (first or secondary) ionization of the molecules or to electron detachment from anions. The alternative strategy of multiple absorption of smaller energy photons suffers from the inherent spreads in absorption statistics. Collisional excitation is possible, as demonstrated with electron collisions with fullerenes [4, 5], but these suffer from a broad energy transfer efficiency, requiring a detailed quantitative analysis of the reaction products with a number of highly non-trivial assumptions.

The origin of the power law behavior is the loss of a

well defined energy scale in the excitation energy distribution caused either by such post-production excitation or by the use of hot sources, which almost unavoidably produce clusters with broad energy distributions. For a unimolecular decay in vacuum, loss of an energy scale is equivalent to loss of a time scale. This is reflected in the absence of a characteristic time scale in the  $1/t$  dependence of the decay rate. If one wants to measure absolute energies under this kind of conditions, it is therefore necessary to introduce an energy scale by hand.

This was done for  $C_{60}^-$  in the experiments reported in [6]. In these experiments, the anions were created hot from the source and injected into an electrostatic storage ring, where they decayed by spontaneous electron emission. At a variable time after production, a small fraction of the un-decayed ions were reheated by one-photon excitation. The photon energy absorbed and dissipated caused a heating of the molecule that led to an enhanced delayed thermal electron emission. The time profile of the enhanced decay was used to locate the equivalent backshifted time, i.e. the time where the spontaneously decaying ions decayed with the same time dependence as the laser excited ions. An overall multiplicative constant on the enhanced decay, which reflects quantities such as laser fluence, beam overlap, and photon absorption cross section was only relevant for the amplitude of the laser enhanced signal and did not enter the analysis.

Together with the instrumental laser firing time, the determination of this apparent shift of the zero time of the power law decay due to the reheating provides the time interval during which one photon energy was lost. The procedure can therefore be used to determine the absolute cooling rate of the ions. The results obtained were in very good agreement with the known facts of  $C_{60}^-$ , such as the electron affinity and also with the model for the radiative cooling developed in [7].

The data from this experiment somewhat surprisingly also allow for the determination of the parameters that determine the energy resolved rate constants. Furthermore, they provide a measure of the relative importance of continuous and discrete cooling. These two types of thermal photon emission differ only by the magnitude of the energies of the photons emitted, and thereby by the effect they have on the measured decay dynamics of the ions.

The demonstration of this is the purpose of this paper.

---

\* klavshansen@tju.edu.cn

The outcome of the analysis of the  $C_{60}^-$  data will provide the absolute decay rate, parametrized by the product of activation energy and heat capacity, the frequency factor of the rate constant, and a binary spectral distribution of the thermally emitted photons.

The remainder of the paper is divided into a section where the theory behind the experimental data and the present analysis is described in some detail. This is followed by a section where the experiments are described, after which a section presents the data analysis and the results. Finally, the procedure and the results are summarized and discussed.

## II. THEORETICAL BACKGROUND

The spontaneous statistical decay of an ensemble of particles in a molecular beam is given by the decay rate averaged over all excitation energies present in the ensemble;

$$R(t) \propto \int_0^\infty g(E)k(E) \exp(-k(E)t)dE. \quad (1)$$

where  $R$  is the measured decay rate, i.e. the number of decays per time unit, and  $k(E)$  is the decay rate constant of an ion with excitation energy  $E$ . The quantity  $g(E)$  is the ensemble density of excitation energy at the time it was created in the source, and  $t$  is the time elapsed from the creation of  $g$  in the source to the measurement. The constant of proportionality is the combined transmission and detection efficiency. When  $g(E)$  is broad, the integrand peaks at the rate constant  $k_m$  for which

$$\frac{d}{dE}k_m(E) \exp(-k_m(E)t) = 0 \Rightarrow k_m(E)t = 1, \quad (2)$$

corresponding to a peak value of  $\exp(-1)/t$  for  $k(E) \exp(-k(E)t)$ . This result is derived without specifying the expression for  $k(E)$  and holds generally, insofar as Eq.(2) has solutions, which may not be the case for ultrafast processes but will be the case for measurement times relevant here. The equation only has one solution if  $k(E)$  is a monotonically increasing function of  $E$ , which can also be safely assumed here.

It is worth demonstrating the generality of the result in Eq.(2) with some different expressions for rate constants. Fig.(1) shows a few examples. The expression for the decay constant, which will also be used in the analysis, is of the simple form

$$k = \omega \exp\left(-\frac{\phi C_v}{E + E'}\right). \quad (3)$$

Here  $C_v$  is the canonical heat capacity in units of  $k_B$ , less one ( $k_B = 1$  will be used throughout), and  $\phi$  is the decay channel activation energy. For thermionic emission from  $C_{60}^-$  this parameter is to a first approximation expected to be the electron affinity of 2.67-2.68 eV [8, 9]. In spite of its simplicity, Eq.(3) is very accurate for our purpose

because only an energy interval of ca. 4 eV is covered in the experiments here. This question is discussed in the appendix and corrections to parameters made in the discussion section.

The rate constants used in Fig.(1) are all variations of the rate constant in Eq.(3). Other examples with different functional forms are given in [3], with an identical conclusion.

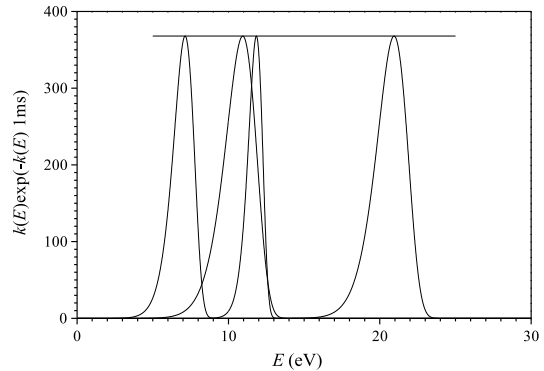


Figure 1. The product of rate constants and survival probability for a broad energy distribution after 1 ms for a few different parameters for the rate constant given in the main text. The line is the calculated value of  $1000/\exp(1) \text{ s}^{-1}$ . The parameters are, from low to high peak energies:  $(\omega, \phi C_v, E') = (10^{14} \text{ Hz}, 434 \text{ eV}, 10 \text{ eV})$ ,  $(10^{12} \text{ Hz}, 434 \text{ eV}, 10 \text{ eV})$ ,  $(10^{14} \text{ Hz}, 300 \text{ eV}, 0)$ , and  $(10^{12} \text{ Hz}, 434 \text{ eV}, 0)$ .

The decay rate is the integral of the peaks in Fig.(1). The width of the peaks are on the order of  $1/d \ln k/de$ . Given the rapid variation of  $k$  with energy, this will remain fairly constant over a wide range of times. This suggests the possibility that also the decay rate may vary approximately as  $1/t$ . The decay rate is most easily calculated by considering the time dependence of the energy distributions. Ignoring the variation of  $g$  with energy, the energy distribution of the surviving ions,  $\exp(-k(E)t)$ , is essentially constant up to an energy close to the value defined by  $k(E) = t$ , at which point it crosses over and rapidly reaches zero. The motion of this cross-over energy with time represents the decay rate. Solving Eq.(3) for  $E$  and deriving with respect to time then gives the decay rate

$$R(t) = -c'g \frac{dE(k=1/t)}{dt} = c'g \frac{\phi C_v}{(\ln(\omega t))^2} \frac{1}{t}, \quad (4)$$

where  $c'$  is a constant that includes the detection, transmission efficiency and other instrumental parameters, and  $g(E)$  is set to a constant,  $g = g(E(k=1/t)) \approx g(E(k=1/t_0))$ . Absorbing  $g$  into the constant,  $c \equiv c'g$ , and rewriting gives

$$\frac{1}{t} = k_{peak} = R(t) \frac{(\ln(\omega t))^2}{c\phi C_v}, \quad (5)$$

where  $k_{peak}$  is the value for which the decay peaks. The difference between the time dependence of the decay rate

and the rate constant at peak decay rate is the time variation of the width of the decaying peak considered a function of excitation energy, and is summarized by the factor  $(\ln(\omega t))^2$ .

In the presence of thermal radiation, which will be present for  $C_{60}^-$  in the experimental data used here, the relation must be reconsidered. In principle also the  $C_2$  emission is a possible channel. However, this has an activation energy which is close to four times that of electron emission from the anion and can safely be ignored. The only channel competing with electron emission is therefore thermal radiation.

In the context of ensembles there are two categories of thermal radiation, defined by the magnitude of the energies of the emitted photons. When the emission is by sufficiently low energy photons, the radiation is effectively a continuous cooling. This means that the energy distribution shifts down with time similarly to the non-radiative situation, just faster. The shape of the cross-over region of the energy distribution is virtually unchanged in this small photon energy limit. When only this type of radiation is present, its effect can be determined from the observed decay rate with an expression analogous to Eq.(5) where  $t'$  is given by

$$R(t) = \frac{cg\phi C_v}{t' \ln(\omega t')^2}, \quad (6)$$

from which the peak rate constant is identified as

$$k(t) = \frac{1}{t'} \quad (7)$$

where  $t'$  is a fictitious time which is equal to the time needed to wait to have an identical decay rate in the absence of radiation. The decay at short times which is not influenced by any radiative cooling can be used to determine the constants of proportionality. In the logarithm the difference between the physical time and  $t'$  can often be ignored.

When large energy photons are emitted, the simple powerlaw relation needs to be modified once more. Photon energies are considered large if the emission of a single photon will quench the decay on a time scale corresponding to the rate constant after emission. The precise energy where this shift from continuous cooling to quenching happens was analyzed in [10], and will be discussed here after the presence of these photons is quantified.

For the fullerenes, the largest part of the radiation is well understood as being carried by the broad surface plasmon resonance [7]. Although centered at 20 eV, it reaches into the near infrared which allows the low energy tail to be excited thermally with an oscillator strength which gives a radiative energy emission rate which is two orders of magnitude higher than the contribution from the vibrational transitions [11]. The calculated magnitude is consistent with both the anion cooling and the original observation of the strong radiative cooling of the much hotter fullerene cation fragments [12]. The distribution of photon energies generated by the plasmon resonance emission covers both the small and large values,

and both types of channels therefore need to be considered in the analysis.

Whereas for small photon energies the emitted power is the relevant quantity, for large photon energies it is the emission rate constant. As photon emission rate constants only vary slowly with the excitation energy of the molecule when compared to the thermionic emission, we can here set the discrete energy emission rate constant to a single value,  $k_p$ . Its presence means that the abundances, and hence also the decay rates, are reduced by the factor  $\exp(-k_p t)$ . Together with the effect of the continuous cooling,  $R_n$ , and after normalization to the short time behavior of  $1/t$  the observed rate is then equal to

$$R_n(t) = \frac{1}{t'} e^{-k_p t} = k(t) e^{-k_p t}, \quad (8)$$

or

$$k(t) = R_n(t) e^{k_p t}. \quad (9)$$

The fitted curve from the experimentally measured spontaneous decay rate of  $C_{60}^-$  from a hot source gives the function [6]

$$R_n(t) = \frac{1}{t} \exp(-122s^{-1}t + 1320s^{-2}t^2), \quad (10)$$

and hence

$$k(t) = \frac{e^{k_p t}}{t} \exp(-122s^{-1}t + 1320s^{-2}t^2). \quad (11)$$

The analysis so far has only dealt with the spontaneous decay. If the molecule is exposed to a laser pulse some time after production, the absorbing fraction of the energy distribution will be shifted up by the photon energy. The situation is illustrated schematically in Fig.(2). The

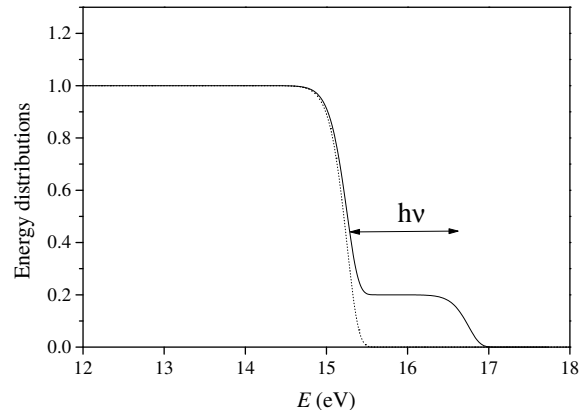


Figure 2. A schematic view of the energy distributions immediately before (dotted line) and after (full line) a photon with energy  $h\nu$  has been absorbed at  $t_{las}$ .

small fraction of the distribution that has been shifted up in energy has almost the same shape as the unshifted distribution had at some earlier time, apart from the absolute height. This has been shown in [13] to which the

reader is referred for details of the calculation. After photon absorption at  $t_{las}$  the decay rate is therefore given by

$$R_{las}(t) = pe^{-k_p(t_{las}-t_0)}R(t-t_{las}+t_0)+(1-p)R(t), \quad (12)$$

where  $t_0$  is a backshifted time, and  $p$  is the photon absorption probability. The backshifted time,  $t_0$ , can be determined by a fit of the first term on the right hand side of Eq.(12) to the decay rate at earlier times. The fraction of absorbing ions,  $p$ , was so low in the experiments that is practically unobservable in the second term in the equation. This facilitated the analysis although it is not an essential requirement. The non-zero value of  $k_p$  has no effect on this part of the analysis. It was not explicitly considered in [6], but the cooling rates obtained there remain unchanged, although it is clear that they only refer to the small photon energy cooling power.

The non-exponential decay is essential to determine the cooling with this procedure because for non-exponential decays the value of both  $p$  (or more precisely  $pe^{-k_p(t_{las}-t_0)}$ ) and  $t_0$  can both be determined, a possibility which is not present for an exponential decay.

As shown, decay rates are proportional to decay constants and Eq.(12) therefore also holds for the peak distribution values  $k_m(t)$  with the substitution  $R(t) \rightarrow k_m(t)e^{-k_p t}$ . The values of  $t_0$  depend on the photon energy and  $t_{las}$  but are independent of the absorption cross section and instrumental parameters. Keeping the laser firing time  $t_{las}$  fixed and varying the photon energy, it is therefore possible to obtain the variation of the rate constant with photon energy as

$$k_m(E(t_{las}) + h\nu) = e^{k_p t_0} R_n(t_0(t_{las}, h\nu)), \quad (13)$$

and similarly

$$k_m(E(t_{las})) = e^{k_p t_{las}} R_n(t_{las}). \quad (14)$$

The energy  $E(t_{las})$  is the energy where the decay rate peaks at time  $t_{las}$ . It is unknown but both  $h\nu$  and  $t_0$  are known. When considering decay rates in the following, the term energy will always refer to this particular energy or the corresponding peak rate energy for the shifted distributions. In statements about the rate constant, the energy will refer to the argument in Eq.(3). Eqs.(13,14) are the basic equations for the analysis of the experimental data.

It should be noted that although a number of measured values of  $t_0$  correspond to times before the mass selection has been completed in these experiments, this causes no problem for the analysis, because other experiments on  $C_{60}^-$  have established the short time behavior as a well behaved power law, see e.g. [11], and this behavior is well established as a general phenomenon, see e.g. the examples listed in [3].

### III. EXPERIMENTS

The data used for the analysis were recorded at the Tokyo Metropolitan electrostatic storage ring, TMU e-

ring. The analysis of the absolute cooling rates derived from these data was published in [6], and the description of the experiment here will be limited to the pertinent points. For a detailed description of electrostatic storage rings and their use for decay measurements, the reader is referred to the rich literature on the subject, see e.g. [14–19].

The  $C_{60}^-$  anions were produced in a laser ablation source without any cooling gas and injected into the ring together with some amount of other anionic carbon species produced during the ablation, mainly other fullerenes. The circulation time of  $C_{60}^-$  in the ring was 122  $\mu s$ . A set of pulsed deflection plates was used to eject the unwanted species, based on their mass dependent circulation time. This beam purification process was completed within 1 ms after production of the ions in the source.

After a variable storage time, the  $C_{60}^-$  beam was exposed to a laser pulse from a tunable optical parametric oscillator (OPO) laser, with photon energies which were varied between 1.9 eV and 2.7 eV in steps of 0.1 eV or 0.2 eV. Pulse energies were kept low, typically a few mJ or lower, to ensure single photon absorption conditions. Spectra were recorded with laser firing times between 4 ms and 35 ms.

Fig.(3) shows two example spectra that were recorded with laser firing time 12.5 ms and photon energies 2.0 and 2.7 eV. Reference spectra without exposure to laser

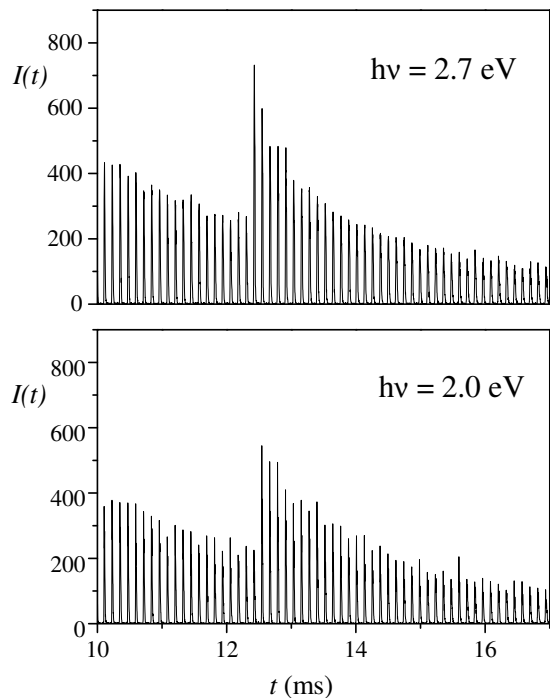


Figure 3. Two spectra with photo-enhanced decays.

light were recorded under identical source and ring conditions, with a timewise interleaving of laser-on and laser-off spectra. The ion source was found to be very stable, with reproducible spontaneous decay rates as a function of time, with variations restricted to minor and slow fluctuations.

tuations in the absolute overall ion intensity. Such source intensity variations were accounted for by a normalization using pre-laser time counts of the laser-on and the laser-off spectra.

The main result of the experiments were the backshifted times of the photo-induced decays. As illustrated with a couple of examples in [6], the photon enhanced signal can be represented well by the expression

$$R_p(t) \propto \frac{1}{t - t_{las} + t_0}, \quad (15)$$

where  $t$  is the time after production of the ions in the source,  $t_{las}$  is the laser firing time, and  $t_0$  the backshifted time. This simple expression only works for situations where, like here, the backshifted time is located in the pure power law sector before radiative cooling modifies the decay. Irrespective of which sector the backshifted time is located, its interpretation is the same, viz. as the reciprocal of the rate constant of the molecule at the energy  $E(t_{las}) + h\nu$ , modified with  $k_p$  as given above.

Fig.(4) shows examples of the fitted  $t_0$  for experiments with two different photon energies and a range of different laser firing times.

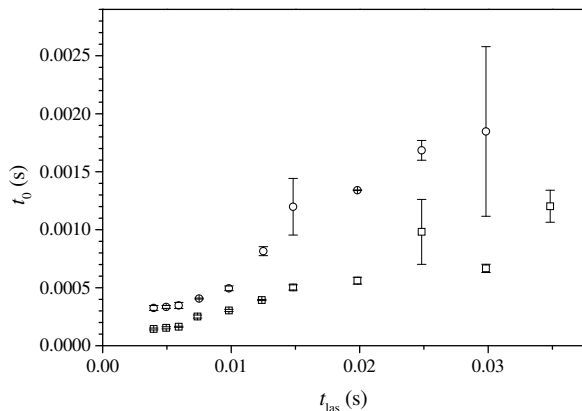


Figure 4. Traces of  $t_0$  as a function of laser firing time measured with the photon energies  $h\nu = 2.0$  eV (circles) and 2.7 eV (squares). The error bars are statistical. Some amount of fluctuation beyond statistical are present, due to the so-called betatron oscillations, a well-known phenomenon from ion storage rings.

#### IV. DATA ANALYSIS

The data analysis proceeds from the data set comprising associated values of laser firing times,  $t_{las}$ , backshifted times,  $t_0$ , and photon energies,  $h\nu$ , together with the rate constants for these times,  $k(E(t))$ , derived from the measured decay rates, as explained above.

The first part of the analysis is initiated by assigning a zero energy arbitrarily to the edge energy,  $E(t_{las})$ , at some given laser time. In this case it was chosen to be  $t_{las} = 0.00994$  s. A few different starting points were

tried without any significant change in the result. The rates at both this times and after absorption of a photon are known, as is the difference in energy. This places all rates measured with the same laser firing time on the energy axis with known relative positions. Such data for different laser firing times are linked to each other when the different  $t_0$ 's are close, ideally identical, for different laser firing times and photon energies. The criterion for two  $t_0$ 's being identical was chosen to be a difference of no more than 10 % in value. The computational procedure is illustrated in Fig.(5). All 62 measured combinations of

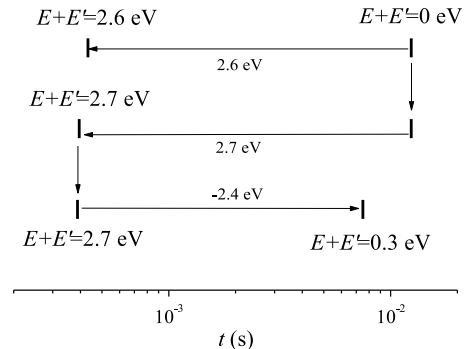


Figure 5. The computational flow in the calculation linking the relative energies, illustrated with three laser firing times, two of which are identical. The energy assignment begins at the top right corner by choosing this as the zero of energy, and flows in the direction of the arrows. As described in the main text, all assigned points can be assigned a known rate constant, modulo the value of  $k_p$ .

laser firing times and photon energies were linked to the common energy reference this way. The linked energies are independent of the values of  $k_p$ , but the rate constants for each time are not. They need to be calculated with Eq.(9).

As the value of  $k_p$  is not known at this point, curves of the thermionic emission rate constant  $k(E)$  were calculated for different assumed values of  $k_p$ , varying it from 10 to 100  $s^{-1}$  in steps of 10  $s^{-1}$ . For each of these, the logarithmic slope was fitted. The logarithmic slope takes the form

$$\frac{d \ln k}{dE} = \frac{\phi C_v}{E^2} = \frac{\ln(\omega/\bar{k})^2}{\phi C_v}, \quad (16)$$

where  $\bar{k}$  is the logarithmic midpoint of the data range for which the derivative is fitted.

The second step in the analysis is taken by considering the variation of the rate constants when the laser time is changed and the photon energy is kept constant. Taking the ratio of the rate constant at the backshifted time to the rate constant at the laser firing time one gets, with

$E_{las}$  denoting the energy edge at the laser firing time,

$$\begin{aligned} \frac{k(t_0)}{k(t_{las})} &= \exp\left(-\frac{\phi C_v}{E_{las} + h\nu} + \frac{\phi C_v}{E_{las}}\right) \\ &\approx \exp\left(\frac{\phi C_v h\nu}{E_{las}^2} - \frac{\phi(h\nu)^2}{E_{las}^3}\right), \end{aligned} \quad (17)$$

or

$$\ln\left(\frac{k(t_0)}{k(t_{las})}\right) \approx \frac{\phi C_v h\nu}{E_{las}^2} \left(1 - \frac{h\nu}{E_{las}}\right). \quad (18)$$

The value of  $E_{las}$  can be expressed in terms of the rate constant as

$$k(t_{las}) = \omega \exp\left(-\frac{\phi C_v}{E_{las}}\right) \Rightarrow E_{las} = \frac{\phi C_v}{\ln(\omega/k(t_{las}))}. \quad (19)$$

Inserting this and taking the square root gives the quasi linear relation

$$\begin{aligned} &\left(\ln\left(\frac{k(t_0)}{k(t_{las})}\right)\right)^{1/2} \\ &= \left(\frac{h\nu}{\phi C_v}\right)^{1/2} (\ln(\omega t_{ref}) - \ln(k(t_{las})t_{ref})) \\ &\quad \times \left(1 - \frac{h\nu \ln(\omega/k(t_{las}))}{\phi C_v}\right)^{1/2}, \end{aligned} \quad (20)$$

where  $t_{ref}$  is a reference time that can conveniently be taken as 1 s.

Repeating this procedure with  $t_{las}$  replaced by  $t_0$  on the right hand side gives a similar result apart from the exchange  $t_{las} \rightarrow t_0$ , and a change of sign on the last term in the last bracket. Averaging the two and dividing by  $\sqrt{h\nu}$  gives

$$\begin{aligned} &\frac{1}{\sqrt{h\nu}} \left(\ln\left(\frac{k(t_0)}{k(t_{las})}\right)\right)^{1/2} \\ &\approx \left(\frac{1}{\phi C_v}\right)^{1/2} \left(\ln(\omega t_{ref}) - \frac{1}{2} \ln(k(t_{las})k(t_0)t_{ref}^2)\right). \end{aligned} \quad (21)$$

When evaluating the quality of this approximation, it was compared with that the ratio of rate constants expressed as

$$\begin{aligned} \ln\left(\frac{k(t_0)}{k(t_{las})}\right) &= -\frac{\phi C_v}{E_{las} + h\nu} + \frac{\phi C_v}{E_{las}} \\ &= \frac{\phi C_v}{E_{las}(E_{las} + h\nu)} = \frac{h\nu}{\phi C_v} \ln\left(\frac{\omega}{k(t_0)}\right) \ln\left(\frac{\omega}{k(t_{las})}\right). \end{aligned} \quad (22)$$

This is inconvenient for graphical representation, but a test using it (not shown) confirms the validity of the above approximation.

Eq.(21) defines a straight line. The value of  $k_p$  enters into the values of  $k(t_0)$  and  $k(t_{las})$  and hence also of the slope and the intercept of the straight line. The intercept squared allows a comparison with the value obtained with Eq.(16) after a correction for the difference between time scales used in the factor  $\ln(\omega t)$  in the two equations. The

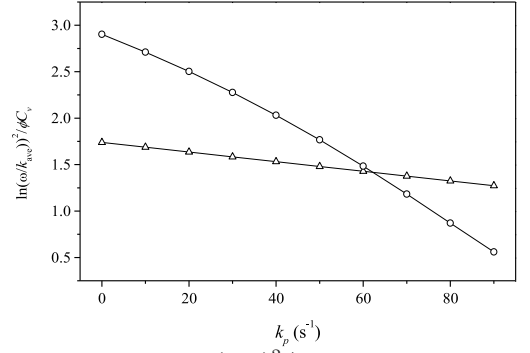


Figure 6. The values of  $\ln(\omega 1s)^2 / \phi C_v$  vs.  $k_p$  calculated with Eq.(16) (circles) and Eq.(21) (triangles).

comparison of the two values is shown in Fig.(6) vs  $k_p$ . Consistency requires identical values for the two curves, yielding the value  $k_p = 60 \text{ s}^{-1}$ . This value inserted into Eq.(21) gives the line in Fig.(7).

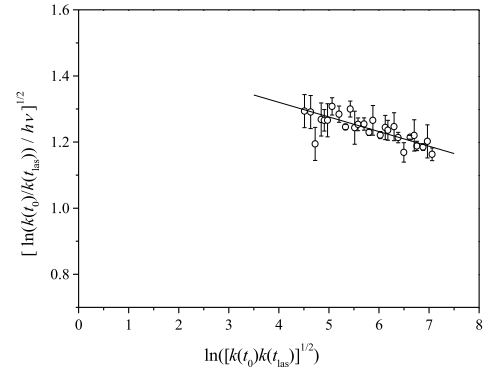


Figure 7. Plot of the data calculated with Eq.(21) and  $k_p = 60 \text{ s}^{-1}$ . The points are grouped in bunches 0.1 wide and the error bars are calculated as the statistical average on the mean. For a few points where there is only one datum in the bunch, the error is set to 0.05.

Another possible contribution to the analysis shown in Fig.(7) should be mentioned. It is obtained by replacing the rate constant at the laser firing time with one for a different photon energy, i.e. using two different photon energies and hence two different backshifted times from the same laser firing time. The equation then reads

$$\begin{aligned} &\frac{1}{\sqrt{h\nu_1 - h\nu_2}} \left(\ln\left(\frac{k(t_0(1))}{k(t_0(2))}\right)\right)^{1/2} \\ &\approx \left(\frac{1}{\phi C_v}\right)^{1/2} \left(\ln(\omega t_{ref}) - \frac{1}{2} \ln(k(t_0(1))k(t_0(2))t_{ref}^2)\right), \end{aligned} \quad (23)$$

where the arguments (1) and (2) refer to different photon energies at the same laser firing time. The present data (not shown) are too scattered to provide any strong confirmation of the analysis, but are consistent with it.

The parameters of the line in Fig.(7) gives the values

$$\ln(\omega 1s) = 33.8 \pm 6.0, \quad \phi C_v = 510 \pm 180 \text{ eV}, \quad (24)$$

corresponding to a frequency factor of  $\omega = 4.9 \times 10^{14} \text{ s}^{-1}$  with a 1- $\sigma$  uncertainty of a factor 400.

The above results can be used to verify the procedure by applying them to the rate constants found with the linking procedure illustrated in Fig.(5). As  $k_p$  is known, also these rate constants are known, apart from the offset in energy. The expression for the rate constant is rewritten, reintroducing the offset energy  $E'$ , as

$$\frac{1}{\ln(\omega/k(E))} = \frac{E + E'}{\phi C_v}. \quad (25)$$

Using the value of  $\omega$  fitted above, the left hand side is plotted vs.  $E$  in Fig.(8). The expected straight line be-

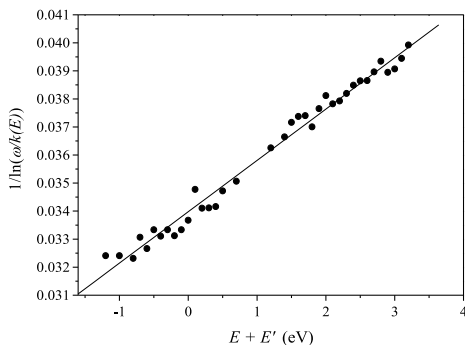


Figure 8. Plot of Eq.(25) with rate constants calculated with the linking procedure explained in the main text, and the value  $k_p = 60 \text{ s}^{-1}$ . The line is a straight line fit. The parameters of the line give the values  $\phi C_v = 546 \pm 12 \text{ eV}$ , and  $E' = 18.6 \pm 0.4 \text{ eV}$ . The error in  $\omega$  is not included in these two standard deviations.

havior is observed, and the fitted value of  $\phi C_v$  is consistent with the previously fitted values, although the uncertainty is significantly larger than the fitted value indicates. The rate constant calculated with the two fit parameters from Fig.(8) and the previously determined  $\omega$  is shown in Fig.(9).

## V. DISCUSSION

The analysis has been based on experimental data and the result in Fig.(9) gives the rate constant from experimental data alone. The different determinations of the parameters can be summarized as a value for the frequency factor of  $\omega = 5 \times 10^{14} \text{ s}^{-1}$  with an uncertainty of a factor 400; two values of  $\phi C_v$  of which  $510 \pm 180 \text{ eV}$  must be considered the primary. The second is consistent with this value but is derived assuming the above value of the frequency factor. Finally, the energy offset for the arbitrarily chosen zero of energy has been fitted to a value of 18.6 eV. The first two parameters in this list have obvious interpretations, but also the energy offset contains information on the reacting species.

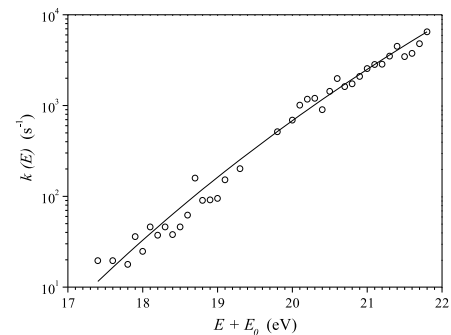


Figure 9. The thermionic rate constant of  $\text{C}_{60}^-$  vs. energy. Error bars can be taken as the average point-to-point fluctuation. The full line are the values calculated with the parameters  $\omega = 4.9 \times 10^{14} \text{ s}^{-1}$ ,  $\phi C_v = 546 \text{ eV}$ , and  $E' = 18.6 \text{ eV}$ . The latter is added to the energy. As it includes the offset in the caloric curves, this is added as  $E_0$ .

The parameters extracted from the fits differ from the values measured in other experiments because approximating a microcanonical rate constant, which is essentially a ratio of level densities with an exponential, will generate some finite size corrections. These corrections were calculated in [20] and can be summarized as

$$C_v = \bar{s} - \frac{\ln(\omega t)^2}{12\bar{s}}, \quad (26)$$

$$\phi = E_a + E_r - E_t, \quad (27)$$

where  $\bar{s}$  is the average of the number of thermally activated oscillators of precursor and product, and the two energies  $E_r, E_t$  are the offsets in the canonical caloric curves for the anion ( $E_r$ ) and the neutral molecule ( $E_t$ ), defined as:

$$E = s_i T - E_i, \quad (28)$$

where  $i$  represents either  $r$  or  $t$ .  $E_a$  is the adiabatic electron affinity with the previously cited value of 2.67 or 2.68 eV.

The correction to the heat capacity is very minor for  $\text{C}_{60}$ , on the order of 1, and can be ignored here. Also the slight variation in the heat capacity due to its temperature dependence will be ignored (see the appendix for this discussion).

The correction to the activation energy is the most important. It vanishes for a harmonic oscillator system if the number and frequencies are identical in the precursor and product, because for harmonic oscillators the offsets are just the sum of their zero point energies. Although the number of oscillators is identical for the anion and the neutral molecule and the oscillators can be considered harmonic because the degree of excitation is very low, a correction arises because the frequencies differ.

The entire sets of frequencies of the neutral and the anion are not known. The two anion infrared active modes

reported in [21] of  $570 \text{ cm}^{-1}$  and  $1374 \text{ cm}^{-1}$  are shifted slightly relative to the neutral values of  $570 \text{ cm}^{-1}$  and  $1411 \text{ cm}^{-1}$  [22]. If the reduction of the highest frequency is used as the scaling for all frequencies, the corresponding reduction in total zero point energy of the anion compared to the neutral is  $0.26 \text{ eV}$ . For this estimate the set of vibrational frequencies of [23] was used. Although these frequencies refer to fullerite and not to gas phase molecules, the values are sufficient for the purpose. The net result is to reduce the effective activation by  $10 \%$ . At the same time the reduced vibrational quantum energies push the heat capacity up toward the classical canonical limit of  $3N - 6$ . The combined effect is therefore less than the  $10 \%$  reduction of the activation energy alone. As the anion spectrum is by and large unknown, a more accurate estimate of the expected value of  $\phi C_v$  will not be attempted.

In the definition of an emission temperature that is used here, some offsets are included into the energy content of the decaying anions [20]. To a sufficient precision the emission temperature is, in terms of the physical excitation energy  $E$  equal to

$$T_e = \frac{1}{C_v} \left( E - \frac{E_a}{2} + E_r \right). \quad (29)$$

The quantity in the bracket is the energy that appears on the abscissa in Fig.(9), i.e. the offset energy  $E_0$  is equal to  $E_r - E_a/2$ . With the reduced frequencies for the anion, this amounts to  $E_0 = 7.7 \text{ eV}$ . To get the physical energy on the abscissa in Fig.(9) this number therefore needs to be subtracted. The rate constant has consequently been determined for the range of energies  $9.7$  to  $14.1 \text{ eV}$ .

The frequency factor can be calculated with an expression given in [20]. It is not an observable that can be compared with other measurable quantities, and as a calculation of it involves a number of factors with each their uncertainty, a calculation of its value will not be attempted here. It should be noted that although the value suffers from a large uncertainty, it is still within the range that must be considered physically reasonable.

Finally, it is worthwhile to consider the amount of radiative cooling by low and high energy photon emission. The distinction between these two categories is made according to whether or not the emission of one photon quenches the electron emission channel. The large photon energy fulfills [10]

$$\begin{aligned} \frac{d \ln k}{dE} h\nu > 1 &\Rightarrow h\nu > \frac{\phi C_v}{(\ln(\omega/\bar{k}))^2} \\ &= \frac{510 \text{ eV}}{\ln(4.9 \times 10^{14}/400)^2} = 0.66 \text{ eV}. \end{aligned} \quad (30)$$

Photons of this magnitude are within thermal reach. The microcanonical temperature of the anion is  $(E + E_0 + E_a/2)/160$ , where  $E + E_0$  is the fitted effective energy content, and  $E_a/2$  is the correction for the finite heat bath, which can be ignored for photon emission. The  $160$  is the heat capacity. This is slightly less than the

contribution from all oscillators, which is  $174$  in the harmonic and high temperature limit. The calculated effective temperature is  $0.12 \text{ eV}$  for the typical energy of  $18 \text{ eV}$ . The phase space of the photon and the quadratic absorption cross section makes the total emission rate depend as the fourth power on the photon energy. In terms of the microcanonical temperature:

$$k_{\text{photon}}(h\nu) d h\nu \propto (h\nu)^4 \frac{e^{-h\nu/T}}{1 - e^{h\nu/T}} d h\nu. \quad (31)$$

The total emitted power is bounded from below by  $0.66 \text{ eV} \times 60 \text{ s}^{-1} = 40 \text{ eV/s}$ . This should be compared with the radiative energy loss of approximately  $100 \text{ eV/s}$  reported in [6]. As discussed, this emitted power refers to the radiation emitted as continuous cooling exclusively. We can use this value to normalize Eq.(31) and find the total emitted power as well as the distribution on low and high energy photons. Using the temperature to  $0.66 \text{ eV}/5.5$ , the low energy photon determines the constant  $c$  as

$$100 \text{ eV/s} = c \int_0^{0.66 \text{ eV}} (h\nu)^5 \frac{e^{-h\nu/T}}{1 - e^{-h\nu/T}} d h\nu. \quad (32)$$

The corresponding high photon energy emission rate constant is

$$k_p = c \int_{0.66 \text{ eV}}^{\infty} (h\nu)^4 \frac{e^{-h\nu/T}}{1 - e^{-h\nu/T}} d h\nu. \quad (33)$$

The value is calculated to  $120 \text{ s}^{-1}$ , i.e. a factor 2 higher than the fitted value. The value decreases to  $90 \text{ s}^{-1}$  for the temperature  $0.11 \text{ eV}$ . Considering that the spectrum in Eq.(31) is somewhat schematic, the agreement is reasonable. In any case, the data suggest that a considerable fraction of the radiative energy is emitted as high energy photons. This is remarkable, both because the systems is as large as it is, and that the electron affinity, which acts as the activation energy and therefore sets the temperature scale, is not particularly large compared with activation energies for unimolecular fragmentation, for example.

## VI. SUMMARY AND PERSPECTIVES

The rate constant for thermal electron emission from  $C_{60}^-$  has been determined over a  $4 \text{ eV}$  energy range. The determination applies a simplified rate constant but does not rely on any modeling. The experimental input is the set of associated values of backshifted times, photon energies and laser firing times in a reheating experiment. The experiment was performed in a storage ring, which is an ion storage device which allows to probe a wide range of times and thereby to cover a reasonable internal energy range.

The analysis provided the absolute value and the logarithmic derivative of the rate constant with respect to

energy, and the product of activation energy and heat capacity, together with the frequency factor for the rate constant. The values were found to be in the range of expected and physical reasonable, although the uncertainties were not negligible. The main problem of the analysis of the data is the presence of betatron oscillations. Although these are inherent to the operation of storage rings, their magnitude decreases in smaller rings, for simple geometrical reasons related to relative detector size. The analysis presented here is a proof of principle for the method which provides rate constants for large systems that are otherwise in practice beyond reach of ex-

perimental measurement, and the commissioning of still smaller storage rings promise the possibility for still more accurate measurements.

## VII. ACKNOWLEDGEMENTS

My coauthors of [6] are gratefully acknowledged for the productive collaboration which provided the experimental material of this paper.

- 
- [1] J. U. Andersen, E. Bonderup, and K. Hansen, *J. Phys. B At. Mol. Opt. Phys.* **35**, R1 (2002).
- [2] K. Hansen, J. U. Andersen, P. Hvelplund, S. Møller, U. Pedersen, and V.V. Petrunin, *Phys. Rev. Lett.* **87**, 123401 (2001).
- [3] K. Hansen, *Rev. Mass Spectrom.* **xx**, xx (2020).
- [4] S. Matt, O. Echt, T. Rauth, B. Dünser, M. Lezius, A. Stamatovic, P. Scheier, and T. D. Märk, *Z. Phys. D* **40**, 389 (1997).
- [5] S. Matt, P. Scheier, A. Stamatovic, H. Deutsch, K. Becker, and T. D. Märk, *Phil. Trans. R. Soc. Lond. A* **357**, 1201 (1999).
- [6] A. E. K. Sundén, M. Goto, J. Matsumoto, H. Shiromaru, H. Tanuma, T. Azuma, J. U. Andersen, S. E. Canton, and K. Hansen, *Phys. Rev. Lett.* **103**, 143001 (2009).
- [7] J. Andersen and E. Bonderup, *Eur. Phys. J. D* **11**, 413 (2000).
- [8] C. Brink, L. H. Andersen, P. Hvelplund, D. Mathur, and J. D. Voldstad, *Chem. Phys. Lett.* **233**, 52 (1995).
- [9] D.-L. Huang, P. D. Dau, H.-T. Liu, and L.-S. Wang, *J. Chem. Phys.* **140**, 224315 (2014).
- [10] P. Ferrari, E. Janssens, P. Lievens, and K. Hansen, *Int. Rev. Phys. Chem.* **38**, 405 (2019).
- [11] J. U. Andersen, C. Brink, P. Hvelplund, M. O. Larsson, B. Bech Nielsen, and H. Shen, *Phys. Rev. Lett.* **77**, 3991 (1996).
- [12] K. Hansen and E. Campbell, *J. Chem. Phys.* **104**, 5012 (1996).
- [13] K. Hansen, *Int. J. Mass. Spectrom.* **430**, 14 (2018).
- [14] S. P. Møller, *Nucl. Instr. Meth. A* **394**, 281 (1997).
- [15] S. Jinno, T. Takao, Y. Omata, A. Satou, H. Tanuma, T. Azuma, H. Shiromaru, K. Okuno, N. Kobayashi, and I. Watanabe, *Nucl. Instrum. Methods Phys. Res. A* **532**, 477 (2004).
- [16] L. H. Andersen, O. Heber, and D. Zajfman, *J. Phys. B: At. Mol. Opt.* **37**, 57 (2004).
- [17] S. Martin, J. Bernard, R. Brédy, B. Concina, C. Joblin, M. Ji, C. Ortega, and L. Chen, *Phys. Rev. Lett.* **110**, 063003 (2013).
- [18] H. T. Schmidt, R. D. Thomas, M. Gatchell, S. Rosén, P. Reinhard, P. Löfgren, L. Brännholm, M. Blom, M. Björkhage, E. Bäckström, et al., *Rev. Sci. Instrum.* **84**, 055115 (2013), URL <http://scitation.aip.org/content/aip/journal/rsi/84/5/10.1063/1.4807702>.
- [19] Y. Nakano, Y. Enomoto, T. Masunaga, S. Menk, P. Bertier, and T. Azuma, *Rev. Sci. Instrum.* **88**, 033110 (2017).
- [20] K. Hansen, *Chem. Phys. Lett.* **620**, 43 (2015).
- [21] P. Kupser, J. D. Steill, J. Oomens, G. Meijer, and G. von Helden, *Phys. Chem. Chem. Phys.* **10**, 6862 (2008).
- [22] L. Nemes, R. S. Ram, P. F. Bernath, F. A. Tinker, M. C. Zumwalt, L. D. Lamb, and D. R. Huffman, *Chem. Phys. Lett.* **218**, 295 (1994).
- [23] J. Menéndez and J. B. Page, *Light Scattering in Solids* (Springer, Berlin, 2000), vol. VIII, chap. Vibrational Spectroscopy of C<sub>60</sub>, pp. 27–95.

## VIII. APPENDIX: THE APPROXIMATION OF THE RATE CONSTANT

The use of Eq.(3) requires that parameters extracted from the experiments need corrections before they can be compared with parameter values from other types of experiments. The corrections are known [20] and will be applied after the analysis.

The energy in the denominator,  $E + E'$ , is the sum of the true thermal energy,  $E$ , and an offset,  $E'$ , which is required to account for situations where the thermal energy is not simply proportional to the temperature. The offset includes the zero point energy of the harmonic oscillators, which provide the largest part of the heat capacity of the molecule, but also accommodates any other thermal offset that may be present below  $E$ , for whatever reasons. In the following this offset will be absorbed into the energy and will not appear explicitly.

The main energy dependence of the electron emission rate constant is the contribution from the ratio of level densities, and the main question therefore concerns the accuracy of the approximation

$$\frac{\rho(E - \phi)}{\rho(E)} = \exp\left(-\frac{\phi C_v}{E + E'}\right). \quad (34)$$

The quality of this approximation is best seen by plotting  $E$  vs.  $\ln(\rho(E - \phi)/\rho(E))$ . From the rewritten relation

$$E = \frac{\phi C_v}{\ln\left(\frac{\rho(E - \phi)}{\rho(E)}\right)} - E' \quad (35)$$

a straight line is expected. It is indeed also seen in Fig.(10). The slope is 434 eV and the offset gives  $E' = 4.64$  eV, both in good agreement with the expected values. Importantly, the line is straight to a good approximation. The value where the expected abscissa is

located is centered slightly below -4, with an  $\pm 2$  eV range at each sides on the ordinate. This is well in the linear part of the curve.

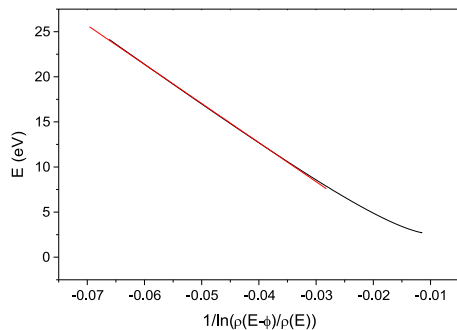


Figure 10. The test of the approximation of the rate constant by the expression in Eq.(34).